The Canadian Mineralogist
Vol. 46, pp. 1511-1526 (2008)
DOI: 10.3749/canmin.46.6.1511

THE STRUCTURE OF "ORTHORHOMBIC" $KAlSiO_4$-*O1*: EVIDENCE FOR Al–Si ORDER FROM MAS NMR DATA COMBINED WITH RIETVELD REFINEMENT AND ELECTRON MICROSCOPY

MIGUEL GREGORKIEWITZ§

Dipartimento di Scienze della Terra, Università di Siena, via Laterina 8, I–53100 Siena, Italy

YING LI AND TIMOTHY J. WHITE

School of Materials Science and Engineering, Nanyang Technological University, 50 Nanyang Drive, Singapore 639798

RAY L. WITHERS

Research School of Chemistry, Australian National University, Canberra ACT 2601, Australia

ISABEL SOBRADOS

Instituto de Ciencia de Materiales, Consejo Superior de Investigaciones Científicas, E–28049 Madrid-Cantoblanco, Spain

ABSTRACT

Dry synthesis of $KAlSiO_4$ at temperatures from 900 to 1500°C yielded products with slightly different powder X-ray-diffraction patterns. "Orthorhombic" $K_xAl_xSi_{2-x}O_4$-*O1* with $x \approx 1$ was obtained as a substantially single phase after heating at 1000°C for one day; we refined its crystal structure from powder X-ray-diffraction data in space group $P12_11$ [MM = 158.17 g/mol, *a* 15.669(2), *b* 9.057(1), *c* 8.621(1) Å, β 90.16(1)°, *V* 1223.5 Å^3, Z = 12, D_x = 2.57 g cm^{-3}, R_B = 0.080]. It is composed of a relatively open [$AlSiO_4$] framework that is a topological variant of tridymite (t) having the supercell (s) metric $\mathbf{a}_s \approx 3\mathbf{a}_t$, $\mathbf{b}_s \approx \mathbf{a}_t + 2\mathbf{b}_t$, $\mathbf{c}_s \approx \mathbf{c}_t$. The space group $P12_11$ allows for Al–Si ordering, and refinement of distance-least-squares restrained models, although problematic owing to the pronounced pseudosymmetry, indicates preference for an ordered pattern where Al and Si are distributed on alternating tetrahedra [*d*Si–O/*d*Al–O = 1.628(1)/1.719(1) Å], so that every SiO_4 tetrahedron is coordinated to four AlO_4 tetrahedra and *vice versa*. The alternating distribution was independently inferred from ^{29}Si and ^{27}Al MAS NMR spectroscopic data, and the framework model obtained from Rietveld refinement with Si on tetrahedron *T*1 could be used to successfully simulate the observed Si(Al_4) doublet peak in the ^{29}Si spectrum. Electron diffraction showed that triple twinning with a rotation of 120° around **c** of the metrically almost hexagonal $P12_11$ cell is ubiquitous and enhances, in the diffraction experiment, the pseudosymmetry inherited from the tridymite subcell. Furthermore, the diffraction aspect of single individuals ($P^*2_1^*$) confirms that the screw axes 2_1-- and --2_1 of the orthorhombic supergroup $P2_12_12_1$ are only approximated.

Keywords: $KAlSiO_4$, kalsilite, kaliophilite, crystal structure, electron microscopy, Rietveld refinement, ^{29}Si MAS NMR, pseudosymmetry.

SOMMAIRE

La synthèse en voie sèche du composé $KAlSiO_4$ entre 900 et 1500°C a donné des produits dont les diagrammes de diffraction X des poudres témoignent des petites différences. La phase $K_xAl_xSi_{2-x}O_4$-*O1* "orthorhombique" avec $x \approx 1$ a été obtenue essentiellement pure après chauffage à 1000°C pour une journée, et sa structure cristalline a été affinée à partir des intensités de diffraction de X sur poudre dans le groupe spatial $P12_11$ [MM = 158.17 g/mol, *a* 15.669(2), *b* 9.057(1), *c* 8.621(1) Å, β 90.16(1)°, *V* 1223.5 Å^3, Z = 12, D_x = 2.57 g cm^{-3}, R_B = 0.080]. Elle est fondée sur une charpente [$AlSiO_4$] relativement ouverte que l'on peut décrire comme variante topologique de la tridymite (t), avec le sur-réseau (s) $\mathbf{a}_s \approx 3\mathbf{a}_t$, $\mathbf{b}_s \approx \mathbf{a}_t + 2\mathbf{b}_t$, $\mathbf{c}_s \approx \mathbf{c}_t$. Le groupe spatial $P12_11$ permet une distribution ordonnée de Al et Si, et l'affinement Rietveld restreint par moindres carrés de distances (DLS), bien que problématique à cause de la forte pseudosymétrie, indique qu'il y a une préférence pour les modèles à distribution alternante [*d*Si–O/*d*Al–O = 1.628(1)/1.719(1) Å] où chaque tétraèdre SiO_4 est lié à quatre tétraèdres AlO_4 et *vice versa*. La distribution alternante a été confirmée par spectroscopie de résonance magnétique nucléaire à haute résolution, obtenue pour les noyaux ^{29}Si

§ *E-mail address*: gregor@unisi.it

et ^{27}Al; le modèle de charpente ayant Si dans le tétraèdre *T*1, issu de l'affinement Rietveld, a été utilisé avec succès pour simuler le pic Si(Al_4) dédoublé observé dans le spectre de ^{29}Si. La diffraction électronique a montré que les macles triples, obtenues par rotation de 120° autour de **c** de la maille $P12_11$ dimensionellement presque hexagonale, abondent et renforcent, dans l'expérience de diffraction, la pseudosymétrie héritée de la tridymite. En outre, l'aspect de diffraction des individus monocristallins ($P^*2_1^*$) confirme que les axes hélicoïdaux 2_1-- et --2_1 du surgroupe $P2_12_12_1$ ne sont que des symétries approximatives.

Mots-clés: $KAlSiO_4$, kalsilite, kaliophilite, structure cristalline, microscopie électronique, affinement Rietveld, RMN MAS de ^{29}Si, pseudosymétrie.

Introduction

Tectosilicates are generated by the apical connection of TO_4 tetrahedra to form three-dimensional networks. A multitude of compositions arise from the complete or partial replacement of Si^{4+} with ions of different valence (*e.g.*, Al^{3+}, P^{5+}) and concomitant charge-balance assured by interstitial cations (*e.g.*, Li^+, Na^+, K^+, Ba^{2+}). Framework topology, topochemistry and conformation are characteristic for a given structure and may change with composition, but quite commonly, there are also polymorphic variations that appear as a function of temperature, pressure or precursor structure (Liebau 1985, Heaney *et al.* 1994). An important tectosilicate structural family is derived from high tridymite, a polymorph of silica with $P6_3/mmc$ aristotype symmetry, in which the unit-cell dimensions are *a* 5.05, *c* 8.26 Å, Z = 4 (Gibbs 1927, Kihara 1978, Nukui *et al.* 1978) and the SiO_4 tetrahedra form six-membered rings circumscribing relatively open channels running parallel to **c** (Fig. 1).

Here we are concerned with the crystallochemical features of a lesser known phase, which has the approximate composition $KAlSiO_4$; its framework topology is a variant to that of tridymite, and it belongs to one of the topological families defined by Smith (1977). This compound, identified as "orthorhombic $KAlSiO_4$-*O1*" by Smith & Tuttle (1957) and "orthorhombic $KAlSiO_4$-*O1* (low T)" by Cook *et al.* (1977), is now known to possess a lower symmetry (Gregorkiewitz 1980). In the present study, it is therefore referred to as "orthorhombic" $KAlSiO_4$-*O1* or $KAlSiO_4$-*O1*. Although natural occurrences are unknown, the material is of considerable importance in the context of high-temperature technologies as it has been found in blast-furnace linings (Rigby & Richardson 1947), magnetohydrodynamic generators (Cook *et al.* 1977) and hazardous-waste incinerator clinkers (Li *et al.* 2003).

Despite its simple formula, $KAlSiO_4$-*O1* suffers from serious problems of pseudosymmetry and twinning, and present knowledge of its crystal chemistry has been limited to an average structure in the orthorhombic space-groups *Pnam* and $Pn2_1m$ (Gregorkiewitz 1980). One can recognize the framework topology, but important details, such as the Al–Si distribution, remain unresolved. A more complete understanding of such details and the polymorphism of $KAlSiO_4$ would be valuable for controlling the formation of $[K_x\square_{1-x}][Al_xSi_{2-x}O_4]$ by-products in incinerators, and more generally, it would permit a greater appreciation of the phase relations in this tectosilicate system.

In the present investigation, $KAlSiO_4$-*O1* was synthesized at different temperatures from dry components and characterized by a combination of X-ray Rietveld structure refinement, selected-area electron diffraction, high-resolution transmission electron microscopy, and magic-angle spinning nuclear magnetic resonance (MAS NMR) spectroscopy, in an attempt to overcome the difficulties with pseudosymmetry through the use of complementary experimental data.

Crystal Chemistry of the Tridymite Family and its Topological Variants

In describing the rings in high tridymite (Fig. 1) according to the orientations of the tetrahedra normal to the basal **ab** plane, one obtains the sequence UDUDUD, where U stands for "apex up" and D for "apex down". Silicates having the same topology of the framework but the crystallochemical formula $[A^+_x\square_{1-x}][B^{3+}_xSi^{4+}_{2-x}O_4]$ ($0 \le x \le 1$, usually $x = 1$) are known as stuffed derivatives of tridymite (Buerger 1954). Although the range of heterovalent substitutions and continuous solid-solutions is extensive, careful examination commonly reveals ordering of the *A*–□ and *B*–Si replacements leading to the formation of commensurate and incommensurate superstructures (Hahn & Buerger 1955, McConnell 1962, Hörkner & Müller-Buschbaum 1979, Nayak & Kutty 1996, Xu & Veblen 1996). Whereas the channels of the aristotype (*e.g.*, high tridymite) are fully expanded, the derivatives usually show a hettotype symmetry that reflects contraction of the channels by TO_4 tilting to satisfy *A*–O bonding requirements. In addition to such conformational changes, frameworks having the same $[A^+_x\square_{1-x}][B^{3+}_xSi^{4+}_{2-x}O_4]$ composition but with topologies distinct from tridymite can arise through a change of the TO_4 orientation sequence (*e.g.*, UUDUDD), which cannot be realized without a disruptive reorganization of the *T*–O bonds (Merlino 1984, Palmer 1994, Andratschke *et al.* 1992, Elfakir *et al.* 1998, Wallez *et al.* 1999). All such permutations were enumerated by Smith (1977), who showed that whereas UDUDUD only yields 6-membered circuits of tetrahedra between the rings superimposed along **c**, the topological variants will produce 4-, 6-, 8-, 10- and even 12-membered loops. The combination of both

mechanisms for structural modification, *i.e.*, conformational and reconstructive change of the framework of tetrahedra, provides for extensive chemical adaptability that can be exploited in the synthesis of materials for catalysis (Hutchings *et al.* 2004), environmental remediation (Gallagher *et al.* 1977), ion exchange and conduction (Minor *et al.* 1978, Gregorkiewitz 1986, Norby & Fjellvåg 1992, Jiménez-Rioboo & Gregorkiewitz 1999) and as electroceramics (Kunimoto *et al.* 2007).

Experimental Procedures

Samples were prepared from stoichiometric $KAlSiO_4$ mixtures of analytical grade K_2CO_3, SiO_2 (amorphous gel) and Al_2O_3 (corundum) powders that were dried at 120°C for four hours, weighed in appropriate proportions, then thoroughly ground mechanically in a zirconia ball mill for three minutes. The mixtures were fired in air over the temperature range 900–1500°C in 100° steps for 1, 3 and 7 days. The products were hand-crushed in an agate mortar and pestle, pressed into Siemens D5005 X-ray diffractometer (XRD) sample holders, and patterns were recorded with Cu$K\alpha$ radiation (λ = 1.540598 and 1.544390 Å) over a 2θ range of 10–137° by step scanning in 2θ increments of 0.02° and fixed counting time of 5 s per step. Rietveld refinements were carried out using both the fundamental parameter (FP) method of Cheary & Coelho (1998) as implemented in TOPAS (2005), and conventional profile-modeling in GSAS (Larson & Von Dreele 1998).

For transmission electron microscopy (TEM), a small quantity of material was crushed in an agate mortar under ethanol, followed by ultrasonic dispersion. Several drops of suspension were deposited on a 3 mm copper grid covered with an amorphous holey carbon foil for examination in a JEM–3010 electron microscope operating at 300 kV and a JEM–100CX at 100 kV. As amorphization was rapid under a focused electron beam, minimum-exposure techniques were used to avoid degradation.

High-resolution solid-state ^{29}Si and ^{27}Al MAS NMR spectra were obtained at 79.5 and 104.3 MHz, respectively, on a Bruker MSL–400 spectrometer working with a magnetic field of 9.4 Tesla and spinning frequencies of about 4 kHz. Chemical shifts δ (in ppm) are given with respect to tetramethylsilane (for ^{29}Si) and 1 M $AlCl_3$ aqueous solution (for ^{27}Al) as external standards.

Results

Phases observed

Figure 2 shows a portion of the XRD patterns for a representative suite of K_2O–Al_2O_3–SiO_2 samples sintered for various times and temperatures. Below 1300°C (especially with longer firing times), the major peaks correspond to (low-T) "orthorhombic" $KAlSiO_4$-*O1* (Kunze 1954, Smith & Tuttle 1957, Cook *et al.* 1977) that became increasingly crystalline at higher temperatures. Almost pure $KAlSiO_4$-*O1* developed at 1000°C for one day, although a trace of Al_2O_3 was found to be invariably present, and at ≥1300°C, leucite ($KAlSi_2O_6$) and other partially characterized $KAlSiO_4$ phases were increasingly evident as volatilization of potassium became significant.

Rietveld refinements of the structure

The diffraction pattern of the material synthesized at 1000°C for one day was selected for detailed Rietveld refinement of $KAlSiO_4$-*O1*. The starting models, with atom positions and isotropic displacement parameters by groups of elements, were taken from Gregorkiewitz (1980). Neutral-atom scattering factors were used; we placed Al in all tetrahedra in those space groups that did not allow for Al–Si order, and soft constraints were applied to the Si–O and Al–O distances. Minor corundum was included as a second phase using standard parameters (IUCr 1984) that were held constant during refinements. A plot of the observed and calculated X-ray-diffraction patterns illustrating the final agreement is given in Figure 3.

Following Gregorkiewitz & Schäfer (1980), the refinement started with the average model in *Pnam* (standard setting *Pnma*), the (orthorhombic) symmetry of highest possible order, and then continued in three orthorhombic and two monoclinic subgroups of index 2 ($Pna2_1$, $Pn2_1m$, $P2_12_12_1$, $P112_1/m$) and index 4 ($P12_11$). Subgroups of equal index have the same order and, therefore, approximately the same number of free parameters. Accordingly, the residuals obtained from Rietveld refinement can be used directly to compare the relative statistical significance of subgroups of the same order, whereas a comparison between space groups of different order requires the application of Hamilton's (1965) test or equivalent criteria. Note also that the symmetry release from *Pnam* to one of the subgroups allows in any case only relatively minor adjustments of the atom positions; the framework topology thus remains the same, defined also through the soft constraints on the Si–O and Al–O distances in the tetrahedra (see above).

The results of these refinement cycles, summarized in Table 1, are quite surprising. Whereas the Bragg residuals R_B are low and decrease slightly for the subgroups (as compared to *Pnam*), the profile residuals R_p and R_{wp} are quite high and almost invariant. Therefore, the apparent improvement of R_B is not supported by statistical criteria (R_{wp} is the relevant residual). The low values of R_B, on the other hand, should correspond to relatively well-refined structures. This unusual situation may be an artefact of inadequate resolution due to pseudosymmetry, as the pseudohexagonal metric with $b^* \approx a^*\sqrt{3}$ (see next section) causes nearly perfect coincidence of reflections with $h + k = 2n$ such as $20l$

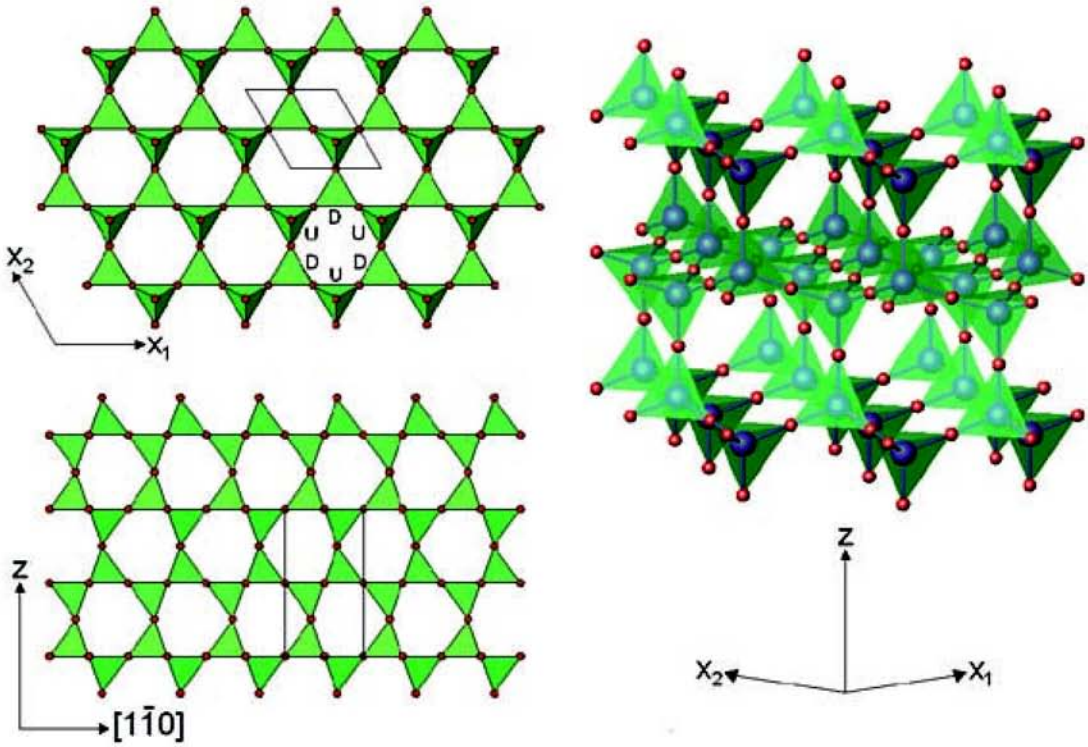

FIG. 1. Polyhedron representation of the structure of high tridymite ($P6_3/mmc$).

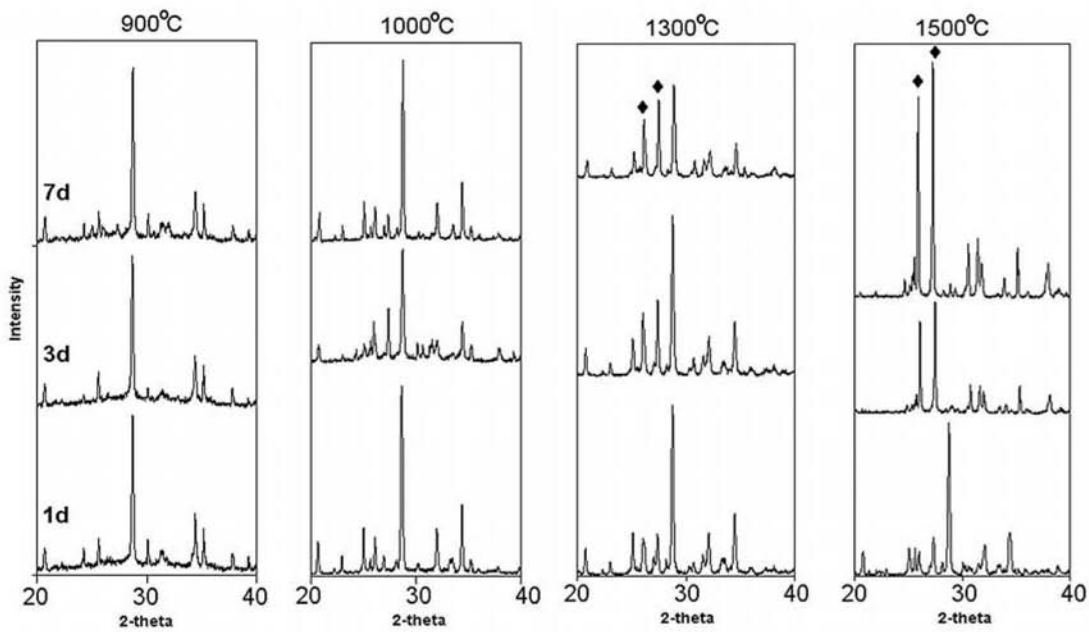

FIG. 2. XRD patterns of samples crystallized at various heating temperatures and times (♦ leucite, $KAlSi_2O_6$).

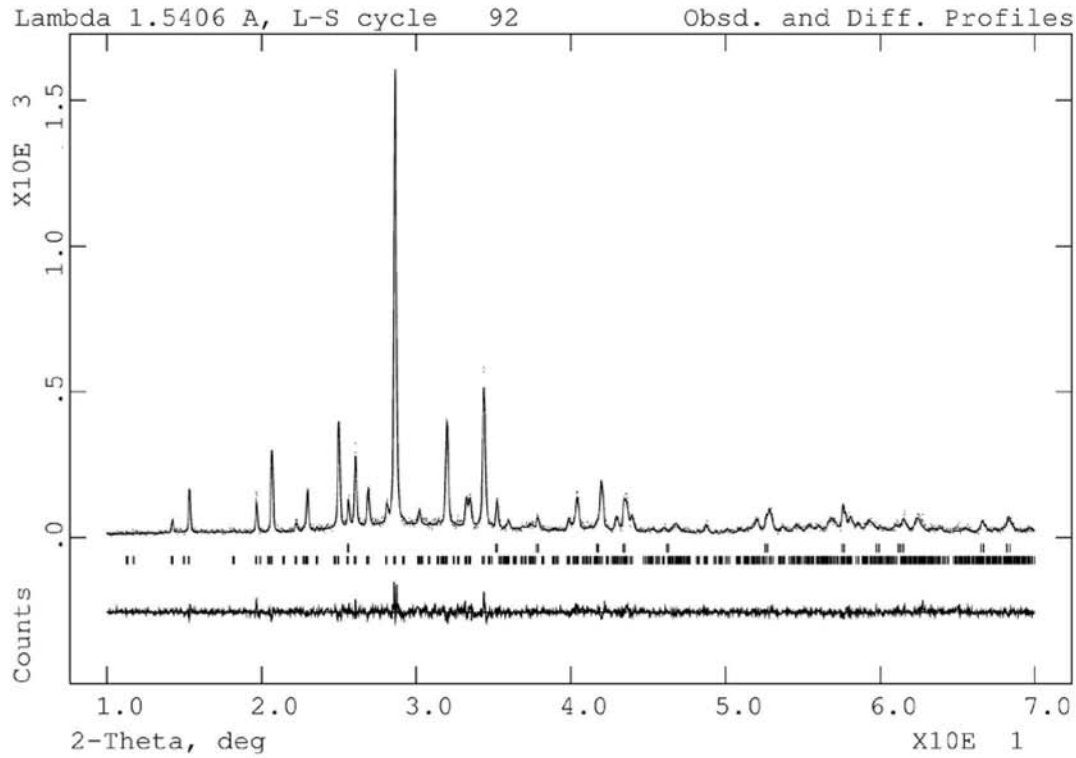

FIG. 3. Observed (dots), calculated (upper line) and difference profiles (lower line), resulting from the Rietveld refinement of the material synthesized at 1000°C for one day. Lower ticks refer to $KAlSiO_4$-*O1* peak positions, upper ticks to corundum.

TABLE 1. UNIT-CELL PARAMETERS AND RESIDUALS OBTAINED FROM REFINEMENT IN DIFFERENT SPACE-GROUPS USING THE FULL X-RAY-DIFFRACTION PATTERN WITH 10° ≤ 2θ ≤ 137°

Space gr. [*i*]	*Pnam* 1	*Pna*2$_1$ 2	*P*112$_1$/*m* 2	*Pn*2$_1$*m* 2	*P*2$_1$2$_1$2$_1$ 2	**P*2$_1$2$_1$2$_1$ 2	*P*12$_1$1 4	**P*12$_1$1 4
a (Å)	15.655(2)	15.656(1)	15.655(1)	15.655(1)	15.659(2)	15.656(2)	15.660(2)	15.660
b (Å)	9.0471(9)	9.0466(8)	9.0467(7)	9.0474(7)	9.0467(9)	9.0466(9)	9.045(1)	9.0450
c (Å)	8.6123(6)	8.6126(6)	8.6115(5)	8.6134(5)	8.6134(7)	8.6128(7)	8.6118(9)	8.6119
β (°)	-	-	90° (fixed)	-	-	-	90° (fixed)	90° (fixed)
R_B (%)	6.3	6.1	6.0	5.9	5.9	5.9	5.0	4.7
R_{wp} (%)	20.5	20.4	20.5	20.8	20.5	20.6	21.5	21.3
R_p (%)	15.7	15.6	15.5	15.9	15.7	15.7	16.7	16.5

* *T*1 = Si. Al and Si are disordered where there is no asterisk. $R_p = \Sigma|Y_o - Y_c| / \Sigma Y_o$, $R_{wp} = \sqrt{[\Sigma w(Y_o - Y_c)^2 / \Sigma w Y_o^2]}$, $R_B = \Sigma|I_o - I_c| / \Sigma I_o$, where Y is the total intensity and I is the diffracted intensity for $KAlSiO_4$-*O1* only.

and 11*l* at low 2θ, or may be due to the increase in peak population at higher 2θ. Since peak overlap due to pseudosymmetry cannot be avoided, we optimized the observed data by imposing a restriction on the 2θ range using the following criteria: the cumulative number of peak positions N_{pos} up to a certain Bragg angle θ can be estimated from

$$N_{pos} = 32\ \pi\ V_{uc}\ \sin^3\theta\ /\ 3\ M_{hkl}\ \lambda^3 \quad (1)$$

which gives, after differentiation, an average distance between neighboring peaks of

$$d2\theta/dN_{pos} = M_{hkl}\ 45\ \lambda^3\ /\ 4\ \pi^2\ V_{uc}\ \sin^2\theta\ \cos\theta\ °2\theta/\text{peak} \quad (2)$$

where M_{hkl} is the multiplicity of a general reflection. Taking M_{hkl} = 8 for the orthorhombic lattice and the unit-cell volume V_{uc} = 1224 Å^3, we can calculate that for $2\theta \geq 60°$, the average distance between neighboring peak positions falls below 0.13°2θ and, for $2\theta \geq 70°$, below 0.10° 2θ. These distances have to be compared with the peak widths which, for a selection of well-resolved peaks in the range from 15 to 30° 2θ, lie in the order of FWHM = 0.13 to 0.15° 2θ. This means that angular resolution is seriously compromised for the region with $2\theta > 60°$ 2θ, where about 84% of all peaks observed up to $2\theta = 137°$ are located.

When the refinements for *Pnam*, $Pn2_1m$, $P2_12_12_1$ and $P12_11$ were repeated by limiting the intensity data to the range $10° \leq 2\theta \leq 70°$, only ~8% of the unresolved high-angle reflections are included. Note (Table 2) that R_p and R_{wp} are now lower and near the expected values for the present dataset, whereas R_B is higher, showing roughly the same tendency as the profile residuals and χ^2 for the four symmetries. Therefore, the significance of the refinement results improved with peak resolution, although all residuals are still quite similar to those of the average model in *Pnam*.

Comparing the results for space groups of order 4 using their residuals alone (Table 2; first entry), $Pn2_1m$ allows for a slightly better model (R_{wp} = 0.157, χ^2 =1.30) than $P2_12_12_1$ (R_{wp} = 0.159, χ^2 in the range 1.32–1.35), but the mirror --*m* (as well as *n*-- and -*a*-) precludes the ordering of Al and Si on alternating tetrahedral sites expected for 1:1 aluminosilicate frameworks (Engelhardt & Michel 1987, Vinograd 1996). Space group $P2_12_12_1$, on the other hand, allows for Al–Si order, and the results for three models show that the one with placement of Si on *T*1 seems superior (R_B = 0.054, χ^2 = 1.32) with respect to models with *T*1=Al (R_B = 0.085, χ^2 = 1.34) or without Al–Si order (R_B = 0.081, χ^2 = 1.35). The comparison of the crystallochemical parameters in Table 2 reveals a similar trend. The dispersion of *T*–O distances and the tetrahedron-distortion index (DITO) are greatest for the average model in *Pnam* (0.21 Å, DITO = 0.0314) and become lower for the subgroup refinements, particularly in the

TABLE 2. RESIDUALS AND SOME CRYSTALLOCHEMICAL PARAMETERS OBTAINED FROM REFINEMENT IN DIFFERENT SPACE-GROUPS USING THE REDUCED DIFFRACTION PATTERN WITH $10° \leq 2\theta \leq 70°$

Order	8	4	4	4	4	2
Space group	*Pnam*	$Pn2_1m$	$P2_12_12_1$	§$P2_12_12_1$	*$P2_12_12_1$	*$P12_11$
T–O restraints (Å)	1.67(3)	1.67(3)	1.67(3)	1.63,1.72(3)	1.63,1.72(3)	1.63,1.72(1)
O–O restraints (Å)	2.74(9)	2.74(9)	2.74(9)	2.66,2.81(9)	2.66,2.81(9)	2.66,2.81(4)
R_B	0.083†	0.076	0.081	0.085	0.054	0.085
	0.095†	*0.086*	*0.112*	*0.108*	*0.111*	*0.080*
R_{wp}	0.162	0.157	0.159	0.159	0.159	0.156
	0.169	*0.161*	*0.170*	*0.168*	*0.169*	*0.157*
R_p	0.122	0.118	0.120	0.120	0.119	0.117
	0.129	*0.121*	*0.130*	*0.129*	*0.130*	*0.116*
χ^2	1.38	1.30	1.35	1.34	1.32	1.51
	1.54	*1.36*	*1.56*	*1.53*	*1.54*	*1.34*
DWD	1.54	1.64	1.60	1.60	1.61	1.66
	1.43	*1.57*	*1.42*	*1.45*	*1.43*	*1.65*
NP	55	86	84	84	84	142
	53	*85*	*83*	*83*	*83*	*145*
T–O or Si–O (Å)	1.59-1.80	1.64-1.74	1.58-1.78	1.55-1.75	1.60-1.70	1.59-1.69
	1.63-1.70	*1.66-1.69*	*1.65-1.68*	*1.60-1.64*	*1.60-1.63*	*1.62-1.64*
Al–O (Å)	-	-	-	1.69-1.79	1.66-1.79	1.63-1.78
	-	-	-	*1.69-1.72*	*1.69-1.73*	*1.71-1.73*
DITO#	0.0314	0.0114	0.0203	0.0201	0.0175	0.0155
	0.0082	*0.0047*	*0.0038*	*0.0041*	*0.0040*	*0.0026*
O–*T*–O (°)	90-127	87-127	91-134	92-133	87-138	88-126
	99-116	*103-114*	*101-119*	*103-119*	*104-116*	*100-116*
V(OTO) (°^{2})	96	64	138	127	164	78
	28	*7*	*15*	*17*	*13*	*9*
T–O–*T* (°)	122-180	124-166	126-171	122-171	124-173	120-170
	127-180	*125-168*	*126-174*	*126-173*	*127-176*	*125-167*

§ *T*1 = Al, * *T*1 = Si, † first entry *T*–O restraints, second entry *T*–O and O–O restraints, # tetrahedron-distortion index (Baur 1974). Al–Si disordered except where indicated. The residual errors R_p, R_{wp} and R_B are defined in Table 1; $\chi^2 = \Sigma w(Y_o - Y_c)^2 / (NO–NP)$. Here, NO stands for the number of observations, and NP represents the number of free parameters.

disordered model in $Pn2_1m$ and the *T*1 = Si model in $P2_12_12_1$ (~0.10 Å, DITO = 0.0114 and 0.0175).

Remembering that the framework topology remains the same in all cases, this result means that $Pn2_1m$ and $P2_12_12_1$ are both suited for minor positional rearrangements to comply with the observed intensities. There is, however, an important difference between the two subgroups, which becomes evident from the crystallochemical parameters. On the one hand, the symmetry release from *Pnam* to $Pn2_1m$ improves the geometry of the tetrahedra (the tetrahedron-distortion index drops from DITO = 0.0314 to 0.0114 and the variance in the tetrahedron angle from *V*(O*T*O) = 96 to 64°^{2}) but leaves the Al–Si distribution disordered; on the other hand, the transition to $P2_12_12_1$ allows for Al–Si order and an improvement of the *T*–O bond distance distortion (DITO = 0.0314 to 0.0175), but the dispersion of the O*T*O angles increases now from *V*(O*T*O) = 96 up to 164°^{2}.

Such deviations from the ideal shape are difficult to reconcile with present knowledge about the rigidity of silicate tetrahedra (Hammonds *et al.* 1994). A new set of refinements has therefore been calculated where restrictions on O–O distances in the tetrahedra were introduced in addition to the *T*–O distance restraints. As expected, the results of these refinements (Table 2, second entry) show that in all cases, the improvement in tetrahedron geometry is achieved at the cost of higher residuals. One interesting observation refers to the bond-length distortion in the tetrahedra, which is now greater for $Pn2_1m$ (DITO = 0.0047) than for $P2_12_12_1$ (DITO in the range 0.0038–0.0041), indicating difficulties to achieve regular tetrahedra of the intermediate size (*T*–O = 1.67 Å) corresponding to Al–Si disorder. The angle variance, on the other hand, remains greater for the models in $P2_12_12_1$ [*V*(O*T*O) in the range 13–17 *versus* 7°^{2} for $Pn2_1m$], indicating that a further release of symmetry is required.

This finding is in agreement with Gregorkiewitz & Schäfer (1980; see also the section below about Pseudosymmetry and Twinning) who pointed out that both $Pn2_1m$ and $P2_12_12_1$ must still be supergroups because the systematic absences for *n*-- and 2_1-- are clearly violated by the presence of weak reflections. In the powder-diffraction pattern, none of these weak reflections is resolved, and initial refinements in $P12_11$, the common subgroup of $Pn2_1m$ and $P2_12_12_1$, were unsuccessful (Table 2, 1st entry). After introduction of the O–O restraints, however, refinement in $P12_11$ converged well, giving a model with clearly lower residuals (R_B = 0.080, R_p = 0.116, χ^2 =1.34). Note that the definition of χ^2 already takes into account NP, the number of free parameters. The decrease from χ^2 =1.36 ($Pn2_1m$, NP = 85) to 1.34 ($P12_11$, NP = 145) indicates therefore that the symmetry release to $P12_11$ is statistically significant.

The corresponding structural improvement is particularly visible in the tetrahedron-distortion index, which drops from DITO = 0.0047 and ~0.0040 in $Pn2_1m$ and $P2_12_12_1$ to 0.0026 in $P12_11$, leaving a geometrically sound and fully ordered model with *d*Si–O = 1.628(1) and *d*Al–O = 1.719(1) Å. A problem arises, however, in the assignment of Si or Al to *T*1 because the parameters for the two alternatives, already very similar for the *T*–O + O–O restrained models in $P2_12_12_1$ (second entry under $^{\S}P2_12_12_1$ and $^{*}P2_12_12_1$ in Table 2) are now virtually identical (represented by $^{*}P12_11$ with *T*1 = Si in Table 2), evidently a consequence of intensity bias due to the orthorhombic pseudosymmetry.

MAS NMR spectroscopy and Al–Si distribution

The strictly alternating Al–Si order is also inferred from ^{29}Si and ^{27}Al MAS NMR spectroscopy (Fig. 4). The ^{29}Si MAS NMR spectra show a clear and reproducible doublet at –85.6 and –88.8 ppm in the intensity ratio of ~2:3, followed, toward the lower fields, by unresolved features that are sample-dependent and probably due to non-crystalline impurities (*cf.* also the spectrum in Fig. 6 of Stebbins *et al.* 1986). As a matter of fact, Rietveld refinement required the introduction of a Debye diffuse scattering term in order to correctly simulate the background with a broad maximum at ~28°2θ, an angle typical for non-crystalline precursors in aluminosilicate syntheses (Madani *et al.* 1990, Shi *et al.* 1996). To test this hypothesis, an estimate of the chemical shift and the spectra expected for ^{29}Si in $KAlSiO_4$-*O1* was made. Using the linear regression equation for δ = f(*TOT*) given by Newsam (1987) and assuming Gaussian peak shapes, simulated spectra could be calculated for the different Al–Si-ordered models obtained from Rietveld refinements. The results showed that the chemical shifts of the maxima adopt, in all cases, δ values in the range –85.3 to –89.1 ppm characteristic for the Si(Al_4) configuration, but the details of the peak shape turned out to depend critically on the particular model. Excellent agreement with observation was obtained for the model in space group $P12_11$ with *T*1 = Si (inset in Fig. 4a), which reproduces a 2:3 doublet at –85.3 and –88.8 ppm and is clearly superior to its alternatives in $P2_12_12_1$, which have a smaller separation of the doublet (*T*1 = Si; 2:3 doublet at –86.8 and 89.1 ppm; *T*1 = Al; 1:2 doublet at 86.5 and 88.9 ppm) or in $P12_11$ with *T*1 = Al, which shows a single peak at –88.7 ppm with a broad shoulder toward higher fields up to about –84.2 ppm. For comparison, synthetic kalsilite shows a single peak at –89.2 ppm, and sodian nepheline $NaAlSiO_4$, with two more distinct crystallographic environments owing to the presence of Na, a 3:1 doublet at –84.5 and –88.5 ppm (Sobrados de la Plaza 1991). Finally, an alternative (although highly improbable) scheme of order that is possible in space group $Pn2_1m$ and contains alternating Al_2O_7 and Si_2O_7 groups can be excluded on the basis of observed data because tentative Rietveld refinements of such models did not converge, and the required peaks for the Si(Al_3Si) and Al($AlSi_3$) configurations at about

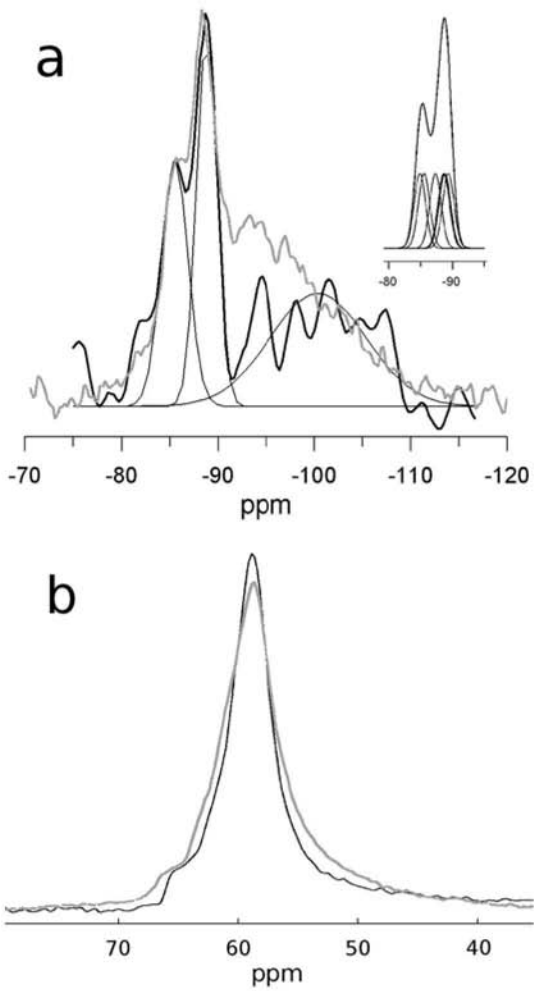

FIG. 4. (a) ^{29}Si and (b) ^{27}Al high-resolution MAS NMR spectra for two different samples of $KAlSiO_4$-*O1*. Grey curves refer to the sample produced from oxides at 1000°C (this work), black curves to a more perfectly crystalline sample obtained from molten salts (Gregorkiewitz 1980). Chemical displacements are given with respect to tetramethylsilane and 1M aqueous $AlCl_3$. The inset in (a) shows a simulated spectrum for the $KAlSiO_4$-*O1* structure (see text).

–93 and 65 ppm, respectively, are not supported by MAS NMR spectroscopy (Fig. 4).

From the present results, the restrained model in $P12_11$ (*T*1 = Si), which also complies with the MAS NMR results, appears the best available solution for the structure of the "orthorhombic" $KAlSiO_4$-*O1* phase. Table 3 gives the atom positions, and Figure 5 shows a projection of the structure along [001] and [010]. Interatomic distances and angles were restrained during refinement, and individual values are therefore not given; their ranges and means can be taken from Table 2 and the accompanying text. The framework topology of $KAlSiO_4$-*O1* is a variant of that of tridymite and its stuffed derivatives. As in tridymite, there are sheets of six-membered rings of $(Al,Si)O_4$ tetrahedra in the **ab** plane, but ring topologies differ from the simple UDUDUD sequence of tridymite. Within the (001) plane, two different types of six-membered oval rings have to be distinguished with respect to the relative orientation of up (U) and down (D) pointing apices of adjacent tetrahedra: UUDUDD (DDUDUU is topologically equivalent to UUDUDD) and UUUDDD, in the proportion 2:1. Subsequent sheets of tetrahedra are connected by bridging apical O atoms and superimpose, owing to the pseudomirror --*m*, in an almost exactly eclipsed manner, leaving 4-, 6-, 8- and 10-membered rings of tetrahedra between adjacent sheets, as opposed to tridymite, which contains only 6-membered rings (Fig. 1).

TABLE 3. FRACTIONAL COORDINATES FOR THE DISTANCE-LEAST-SQUARES-RESTRAINED MODEL OF THE $KAlSiO_4$-*O1* STRUCTURE OBTAINED FROM RIETVELD REFINEMENT IN SPACE GROUP $P12_11$, ALLOWING FOR Al–Si ORDER (*T*1 = Si)

site	*x*	*y*	*z*	U_{eq}/pm²
Si1	-0.2749(19)	0.343(4)	0.5480(33)	290(40)
Al2	-0.2756(21)	0.340(5)	-0.0688(34)	
Al3	-0.1111(16)	0.169(5)	0.4311(34)	
Si4	-0.1127(16)	0.160(5)	0.0458(34)	
Si5	0.0581(17)	0.336(5)	0.5531(35)	
Al6	0.0566(19)	0.331(5)	-0.0602(36)	
Al7	0.2350(20)	0.179(5)	0.5669(36)	
Si8	0.2334(18)	0.176(5)	-0.0519(35)	
Si9	0.4031(17)	0.331(5)	0.4488(34)	
Al10	0.4043(18)	0.328(5)	0.0713(34)	
Al11	0.5666(21)	0.162(5)	0.5507(37)	
Si12	0.5644(19)	0.162(5)	-0.0624(36)	
O1	-0.2062(23)	0.211(5)	0.5185(52)	130(50)
O2	-0.2039(21)	0.199(6)	-0.0358(50)	
O3	-0.0329(22)	0.295(6)	0.4729(51)	
O4	-0.0436(23)	0.287(6)	0.0049(53)	
O5	0.1338(21)	0.224(6)	0.5030(51)	
O6	0.1351(19)	0.212(6)	-0.0003(50)	
O7	0.3021(18)	0.288(6)	0.4603(48)	
O8	0.2992(21)	0.276(6)	0.0486(48)	
O9	0.4600(22)	0.207(6)	0.5364(51)	
O10	0.4652(21)	0.202(6)	-0.0276(54)	
O11	0.6338(22)	0.293(6)	0.4736(47)	
O12	0.6299(22)	0.282(6)	0.0132(46)	
O13	-0.0839(28)	0.000(5)	0.5074(49)	
O14	-0.0801(29)	0.001(5)	-0.0182(48)	
O15	0.2433(31)	-0.008(5)	0.5385(52)	
O16	0.2454(32)	0.000(5)	-0.0223(54)	
O17	0.5868(30)	-0.008(5)	0.4719(47)	
O18	0.5865(29)	0.000(5)	0.0086(46)	
O19	-0.2844(28)	0.371(6)	0.7344(32)	510(70)
O20	-0.1267(26)	0.155(6)	0.2335(32)	
O21	0.0449(26)	0.331(6)	0.7412(34)	
O22	0.2443(28)	0.211(5)	0.7634(34)	
O23	0.4294(24)	0.333(6)	0.2659(33)	
O24	0.5778(26)	0.158(6)	0.7501(35)	
K1	-0.2943(19)	0.0280(13)	0.247(5)	370(40)
K2	-0.2086(18)	-y(K1)*	0.740(6)	
K3	0.0750(21)	-0.0103(50)	0.754(6)	
K4	0.1033(21)	0.0129(57)	0.253(7)	
K5	0.3979(19)	-0.0159(57)	0.748(7)	
K6	0.4545(17)	-0.0045(44)	0.252(6)	

* used to fix origin on *y*. Range of observed data $10° \le 2\theta \le 70°$, $R_B = 0.080$, $R_{wp} = 0.157$, $R_p = 0.116$, $\chi^2 = 1.34$.

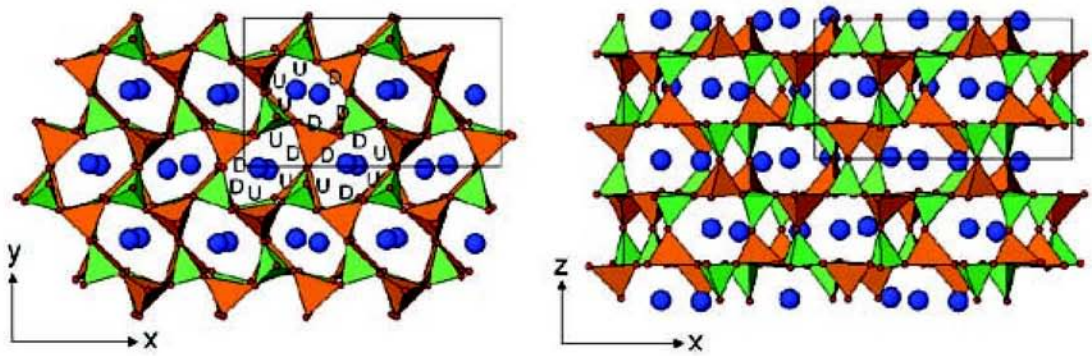

FIG. 5. Projections of the structure of $KAlSiO_4$-*O1* with orderly distributed SiO_4 (green) and AlO_4 (red) tetrahedra.

Pseudosymmetry and twinning

A more detailed knowledge about the intriguing problems with pseudosymmetry and space-group ambiguity was obtained from electron diffraction and microscopy. Whereas the true local symmetry of $KAlSiO_4$-*O1* is orthorhombic or lower, the deviation from the underlying hexagonal parent metric is very slight, *e.g.*, $a_t = a_s/3 = 15.669/3 = 5.2230$ Å *versus* $|(\mathbf{a}_t + 2\mathbf{b}_t)|/\sqrt{3} = b_s/\sqrt{3} = 9.057/\sqrt{3} = 5.2291$ Å. Note that $(5.2291–5.2230)/5.2260 \approx 0.1\%$ is undetectable in typical electron-diffraction patterns. This minimal distortion favors the common occurrence of triple twinning observed in selected-area electron-diffraction patterns (EDPs). Figure 6a, for example, shows a triply twinned crystal viewed along $[0001]_t \equiv [001]_s$, whereas Figure 6b contains a corresponding single-domain microdiffraction pattern. Regarding intensities, the single-domain EDP clearly shows *pmm* symmetry, although the subcell reflections are dominant and approximately obey a *p*6 symmetry (*e.g.*, the set $01\bar{1}0_t$ – $10\bar{1}0_t$, *etc.*, complies with *p*6, the set $02\bar{2}0_t$ – $20\bar{2}0_t$ does less so). By triple twinning, all reflections $hk0_s$ with $h + k = 2n$ will superimpose so that their intensities tend to follow *p*6 symmetry if the twin is made up of three individuals of equal volume. Note that Figure 6a is dominated by an individual oriented as in Figure 6b. Reflections with $h + k = 2n + 1$ will not superimpose, but twin equivalents appear at positions that violate the orthorhombic reciprocal cell defined by the first individual.

This propensity for twinning is ubiquitous and makes space-group determination by EDPs a challenging exercise. Figure 7a is a typical <110>$_t$ zone-axis pattern in which $[1\bar{1}00]_t^* \equiv [3\bar{1}0]_s^*$ and the three-fold-symmetry-related parent reflections are $[\bar{1}010]_t^* \equiv [\bar{3}10]_s^*$ and $[01\bar{1}0]_t^* \equiv [020]_s^*$. The near-perfect hexagonal metric means that the strong parent reflections in the Zero-Order Laue Zone (ZOLZ) at the corresponding $[130]_s$, $[\bar{1}30]_s$ and $[100]_s$ zone-axis orientations overlap perfectly. The much weaker satellite reflections, however, may well occur in only one or other of these orientations.

Microdiffraction patterns (*cf.* Figs. 7c,d in particular), taken with a small condenser aperture to illuminate a much smaller area than conventional selected-area EDPs while still retaining relatively high reciprocal-space resolution, indeed suggest that the EDP in Figure 7a is a twinned composite. The relative intensity of the two sets of satellite reflections in Figures 7a,b change rapidly as the electron beam is moved, as expected for relatively fine-scale twinning. Under these conditions, it was difficult to test the validity of the *n*-- rule for systematic absences visible in Figure 7c. Nevertheless, although it was possible to obtain single-crystal images for the orientation shown in Figure 7d, even the most carefully selected single-crystal images taken along $[100]_s$ were found to contain small traces (quite weak in Fig. 7c) of the second type of satellite reflections, the ones that occur in Figure 7d, suggesting a slight violation of the glide plane *n*--, in agreement with the results obtained from an X-ray single-crystal study (Gregorkiewitz 1980).

In the case of the remaining major zone-axis orientation, *i.e.*, $[010]_s$ (see Fig. 8a), twinning may again be present, but it cannot explain the presence of $h0l_s$, *h* odd, reflections. The presence of $h0l_s$, *h* odd, reflections at this $[010]_s$ zone-axis orientation is incompatible with an *-a-* glide perpendicular to $\mathbf{b}_s$ and thus rules out *Pnam* or $Pna2_1$ as potential resultant space-group symmetries, although *Pnam*, which is a minimal supergroup of $Pn2_1m$ and $P2_12_12_1$, might be valid as an approximately fulfilled pseudosymmetry, in accordance with the results of the Rietveld refinements. It is also interesting to note that the intensities along the row $00l$ are mostly low for $l = 2n + 1$ (the condition for $--2_1$ and, partially, for *n*--), whereas the row $h00$ has quite strong reflections violating $h = 2n$ (condition for 2_1-- and, partially, for

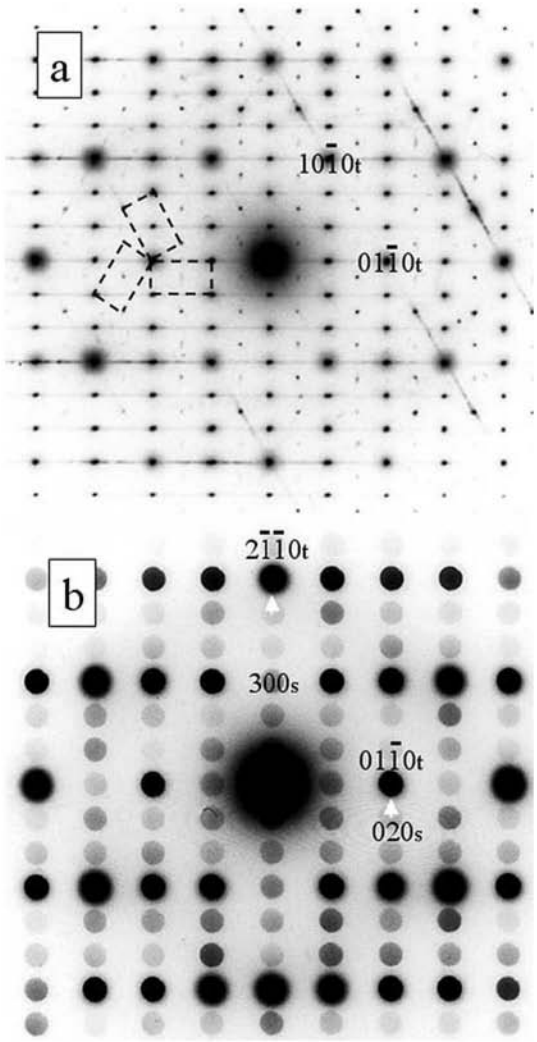

FIG. 6. (a) Electron-diffraction pattern of a triple twin of $KAlSiO_4$-*O1* and (b) microdiffraction pattern of a single individual. Indexation is with respect to the orthorhombic supercell (s) and the hexagonal tridymite-type parent subcell (t) defined by the relation $\mathbf{a}_s = 3\mathbf{a}_t$, $\mathbf{b}_s = \mathbf{a}_t + 2\mathbf{b}_t$, $\mathbf{c}_s = \mathbf{c}_t$; $\mathbf{a}_s^* = {}^1/_6\,[2\bar{1}10]_t^*$, $\mathbf{b}_s^* = {}^1/_2\,[01\bar{1}0]_t^*$, $\mathbf{c}_s^* = \mathbf{c}_t^*$. In the triple twin (a), the near-hexagonal metric is clear from the absence of splitting of the parent reflections. The three individual orthorhombic reciprocal-lattice unit-cells are marked by the dashed lines. Viewing direction is $\mathbf{c}_s = \mathbf{c}_t$ in both cases.

-a-). It thus appears that both $Pn2_1m$ and $P2_12_12_1$ must still be pseudosymmetries, but the symmetry release from *Pnam* to $Pn2_1m$ is better suited to adjust those atomic positions where averaging over pseudosymmetry-related sites is inconsistent with intensities.

Note that $P12_11$ is a common subgroup of $Pn2_1m$ and $P2_12_12_1$ and allows release of the pseudosymmetry plane *--m*, which arises from the similarity of the X-ray scattering power of Al and Si, as well as the more intensity-offending screw axis 2_1--. Convergent-beam patterns (see Fig. 8b) confirm the systematic absence condition for -2_1- ($F[0k0]_s = 0$ unless k = even), but Figure 8a does not show an appreciable departure of the angle β from 90°. A deviation from Laue symmetry *mmm* is therefore hardly visible in powder diffraction, which contributes to the difficulties encountered for the refinement in space group $P12_11$ (see discussion of Table 2 above).

The origin of the streaking evident in Figure 6a along $\mathbf{b}_s^*$ for the twin individuals can be observed directly by HRTEM, in which extended defects are common (Fig. 9). Although the collection of such images was problematic owing to damage by the electron beam, a possible interpretation is that at the boundaries, the oval six-membered rings are replaced by one of their conformational or topological alternatives. Alternatively, or in addition, there might be a variation in the Al–Si distribution and a corresponding adjustment of the local K stoichiometry, leading to distinct image-contrast. Certainly, such defects are likely to be common in $KAlSiO_4$-*O1*, as several single-crystal X-ray-diffraction patterns (Gregorkiewitz 1980) also show diffuse intensity along $\mathbf{b}_s^*$.

DISCUSSION

Structure and polymorphism

At least ten different polymorphs have been reported for compositions near $KAlSiO_4$. For the present purpose, we consider six groups: (i) the kalsilite family, (ii) megakalsilite, the synthetic (iii) *O1*, (iv) *O2* and (v) *Icmm* phases, and (vi) kaliophilite. Kalsilite ($KAlSiO_4$, Perrotta & Smith 1965) and its relatives trigonal kalsilite ($KAlSiO_4$, Cellai *et al.* 1997), trikalsilite ($Na_{0.3}K_{0.7}AlSiO_4$, Bonaccorsi *et al.* 1988) and tetrakalsilite ($Na_{0.2}K_{0.8}AlSiO_4$, Merlino *et al.* 1985), are all based on an [$AlSiO_4$] framework having the tridymite topology. Megakalsilite ($KAlSiO_4$, Khomyakov *et al.* 2002) and $KAlSiO_4$-*O1* (Gregorkiewitz 1980) are topological variants of tridymite, with UDUDUD and UUUDDD rings in the ratio 1:3 in megakalsilite, and UUDUDD and UUUDDD rings in the ratio 2:1 in $KAlSiO_4$-*O1*. For the high-T variant of $KAlSiO_4$-*O1* as well as the remaining groups ($KAlSiO_4$-*O2*, $KAlSiO_4$-*Icmm* and kaliophilite), the crystal structures are yet to be resolved, but there is little doubt that the *Icmm* phase, which can be synthesized from $RbAlSiO_4$-*Icmm* (Minor *et al.* 1978) or $CsAlSiO_4$-*Icmm* (Gregorkiewitz 1986) through ion exchange at low temperatures, is based on the framework of $RbAlSiO_4$ (Klaska & Jarchow 1975), which exhibits UUUDDD rings and the topological symmetry *Icmm*.

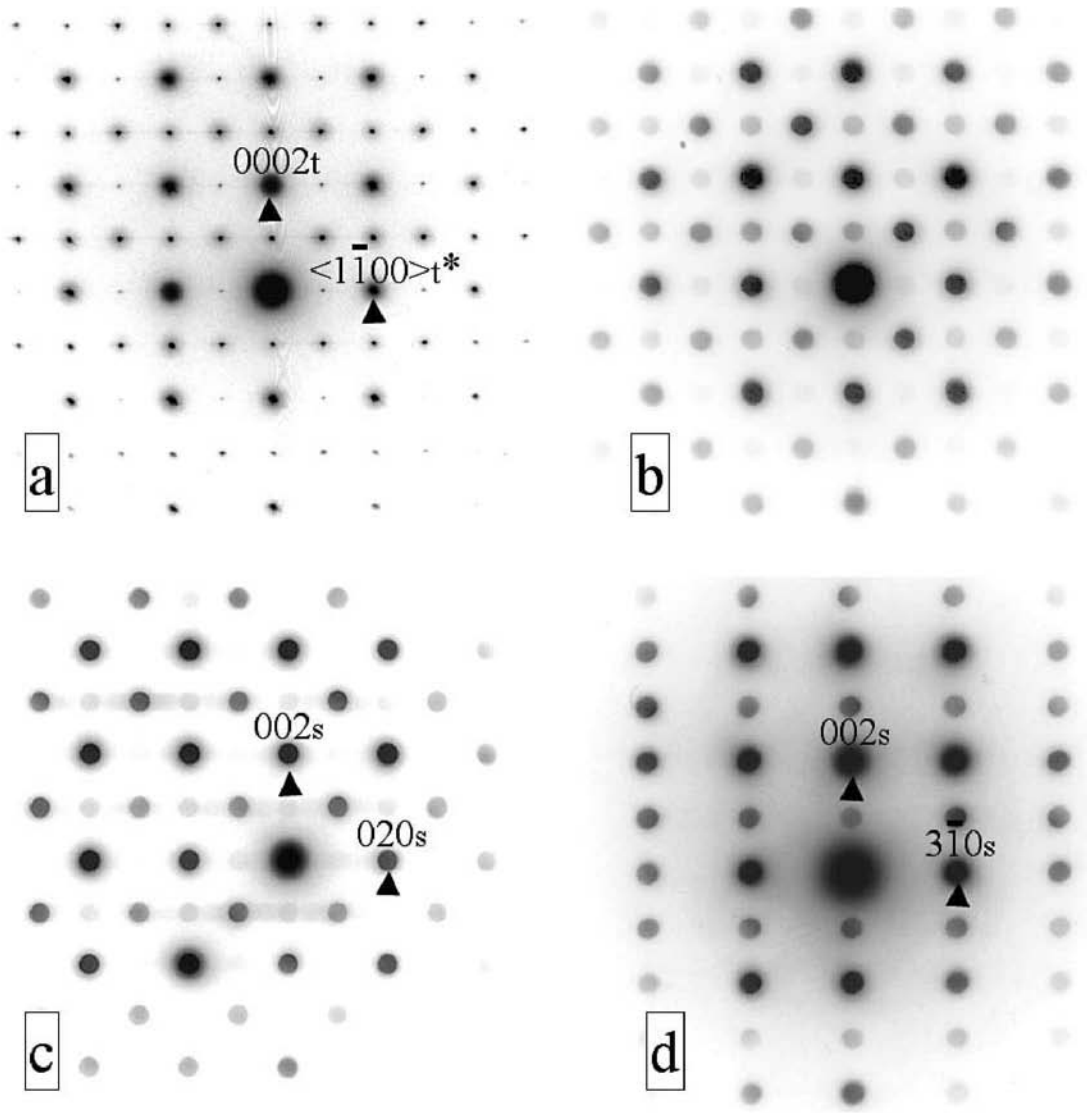

FIG. 7. (a) An average electron-diffraction pattern from a large area, and (b), (c), (d) microdiffraction of small single-domain regions. Patterns (a) and (b) pertain to a twin, (c) and (d) to single individuals. Viewing direction is along $<110>_t$ equivalent to either $[100]_s$, $[130]_s$ or $[\bar{1}30]_s$ in (a) and (b), along $[100]_s$ in (c) and along $[130]_s$ in (d).

Although the different phases can be distinguished by their cell parameters, care has to be taken in the interpretation of powder-diffraction patterns, where the pronounced pseudosymmetry inherited from the underlying tridymite cell may allow for alternative, nonequivalent parameters. One example is the "orthorhombic" $3\boldsymbol{a}_t$ (15.67 Å), $\boldsymbol{a}_t + 2\boldsymbol{b}_t$ (9.06 Å), $\boldsymbol{c}_t$ (8.62 Å) cell of $KAlSiO_4$-*O1*, which is metrically equivalent to a hexagonal cell with $2\boldsymbol{a}_t + 4\boldsymbol{b}_t$ (18.1 Å), $\boldsymbol{c}_t$ (8.62 Å), and not to be confused with the (truly) hexagonal cell of megakalsilite of the same dimensions. In the present case, the hexagonal alternative can be excluded by electron diffraction (Figs. 6–8), which clearly confirmed the "orthorhombic" cell for the $KAlSiO_4$-*O1* phase.

To check the identity of our material in more detail, the exact unit-cell dimensions for various known $KAlSiO_4$-*O1* samples are compared in Table 4. Differences in a and b are small for values derived from

single-crystal or Rietveld cell refinements (the last four entries), and the more important deviations in the first three entries are hardly significant, considering that the pseudohexagonal metric allows for alternative indexing of half of all reflections (those of parity $h + k = 2n$). A significant difference (~50σ), however, seems to exist for the c parameter, which is larger for our material (8.62 Å) when compared with the first four entries in Table 4 (8.57 Å). The c parameter reflects Al–O–Si angles along and the tilting of tetrahedra against the normal on the six-ring sheets, with the maximum (8.69 Å in kalsilite, Perrotta & Smith 1965) corresponding to straight Al–O–Si groups and no tilting. The large value in our material may reflect a higher degree of disorder that prevents the tetrahedra from attaining maximum tilts. This would be in line with earlier findings about the thermal expansion behavior of c in $KAlSiO_4$ (Henderson & Taylor 1988, Sandomirsky & Urusov 1988, Capobianco & Carpenter 1989), showing that in kalsilite, c shrinks with increasing temperature, whereas in $KAlSiO_4$-*O1*, c expands up to a temperature between about 500 and 800°C in a sample-dependent fashion.

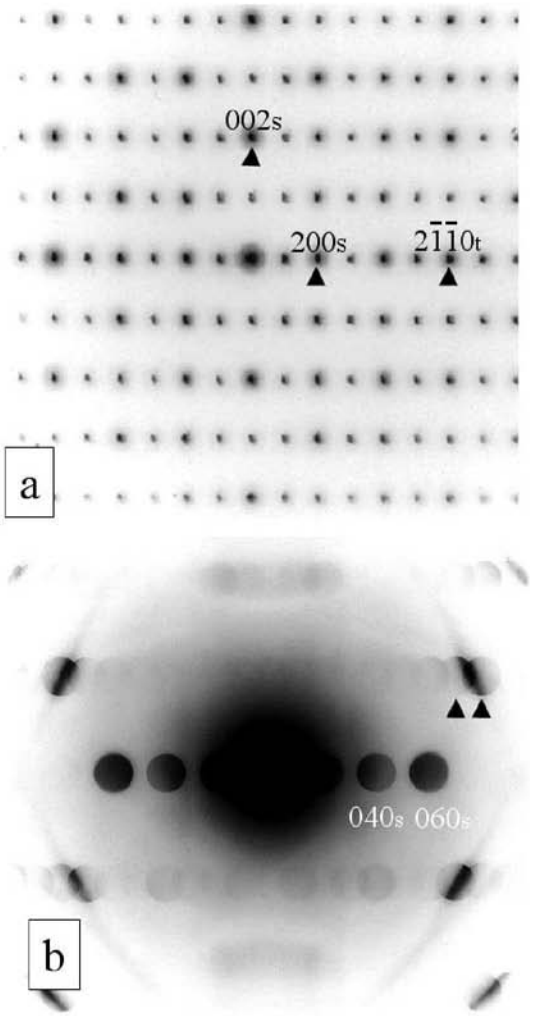

FIG. 8. (a) A $[010]_s$ selected-area diffraction pattern and (b) a convergent-beam pattern in which the $[0k0]_s$* row confirms the systematic absence condition $F[0k0]_s^* = 0$ unless k is even.

Symmetry and order of Al and Si

In contrast to the present results, structure refinement using single-crystal data (Gregorkiewitz 1980) has shown that the lowest residual errors for the average structure of $KAlSiO_4$-*O1* are obtained in $Pn2_1m$. In this space group, owing to the presence of --*m*, no alternating Al–Si scheme of order is possible. As mentioned above, in stoichiometric $KAlSiO_4$ compositions with an Al:Si = 1:1 ratio, Loewenstein's (1954) rule is expected to hold, giving full order with alternating Al and Si tetrahedra. Actually, all known structures of $KAlSiO_4$ (see preceding section) show alternating Al–Si order, and both Rietveld refinement and the comparison of observed and calculated ^{29}Si MAS NMR spectra (see discussion of Fig. 4 above) confirm that the alternating order is also realized in $KAlSiO_4$-*O1*.

The Rietveld refinements were biased by pseudosymmetry at various levels. Space group *Pnam* represents the symmetry of the framework topology, and refinement in this space group results in a relatively well-defined average structure ($\chi^2 = 1.38$, Table 2), in which the averaging implies Al–Si disorder (*i.e.*, Al = Si by virtue of the mirror --*m*) and sets constraints on the tilting of tetrahedra, which leads to a poor geometry in several places. For example, one *TOT* angle, by virtue of the center, $\bar{1}$, becomes 180° (highly improbable in tectosilicates: Liebau 1985), and the variance of the tetrahedron angle *V*(*OTO*) remains relatively high even in the more restrained refinement ($28°^2$, Table 2). The stepwise release of symmetry down to $P12_11$ proved appropriate to arrange for both of these aspects (Al–Si order and geometry of the tetrahedra), but it was only barely backed by observed intensities owing to the pseudohexagonal metric (only reflections *hkl* with $h + k = 2n + 1$ are free of systematic coincidences), the weakness of the reflections violating the glides (*n*--, -*a*-) and screws (2_1--, --2_1) and, most importantly, the pseudo-orthorhombic metric ($\beta = 90.16°$), which causes all reflections *hkl* to coincide with –*hkl*, the nonequivalent counterpart in monoclinic symmetry.

As a consequence, refinement in the subgroups of *Pnam* showed only small variations in the residual errors, and a significant part of discrimination between the different models relies on the statistical analysis of crystallochemical parameters [DITO, *V*(*OTO*); Table 2], particularly those obtained after introduction of more stringent distance-least-squares (DLS) restraints. Even

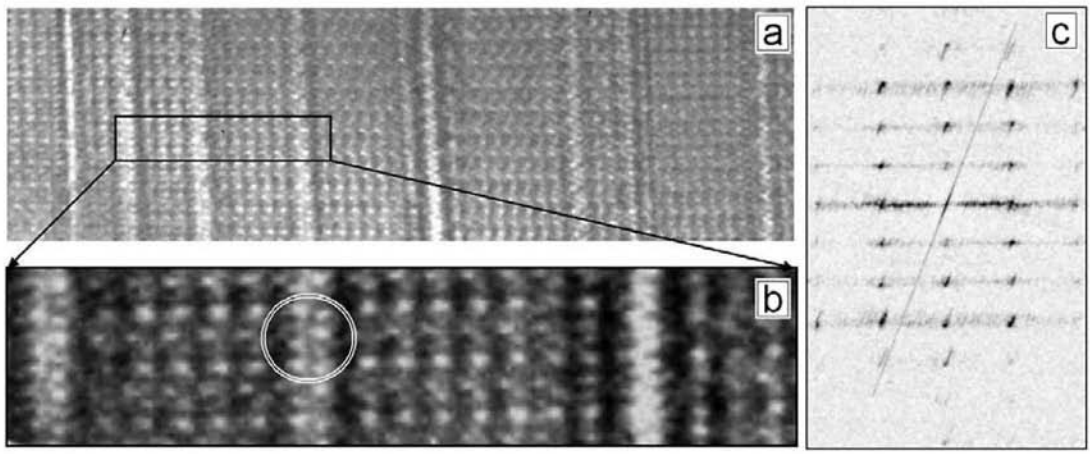

FIG. 9. (a) HRTEM image of a single individual containing extended defects. (b) Enlargement providing detail of three boundaries. The contrast surrounding the extended defects is not directly interpretable but may correspond to the incorporation of channels of different dimensions or a local variation in the Al:Si ratio that must be charge-balanced by the presence of nonstoichiometric K or vacancies. (c) Fourier transform obtained from the whole high-resolution image (not shown). Note the streaks of diffuse intensity perpendicular to the boundaries and the similarity to the diffraction pattern in Figure 6a.

TABLE 4. COMPARISON OF UNIT CELLS FOR VARIOUS SAMPLES OF $KAlSiO_4$-*O1*

reference	symmetry[1]	*a* (Å)	*b* (Å)	*c* (Å)
Kunze (1954)	$P^*2_12_1$	15.671(2)[2]	9.012(2)[2]	8.573(2)[2]
Smith & Tuttle (1957)	-	15.69	9.06	8.562
Cook *et al.* (1977)	$P^*2_12_1$	15.642(2)	9.057(2)	8.582(2)
Gregorkiewitz (1980)	$P^*2_12_1$	15.67(1)	9.07(1)	8.560(5)
this work 2θ ≤137°	$P2_12_12_1$ (*T*1 = Si)	15.656(2)	9.0466(9)	8.6128(7)
this work 2θ ≤70°	$P2_12_12_1$ (*T*1 = Si)	15.674(2)	9.0570(9)	8.6221(7)
this work 2θ ≤70°	$P12_11$ (*T*1 = Si) *T*–O + O–O restrained	15.669(2)	9.0571(9) β = 90.16(1)°	8.6211(6)

[1] Diffraction aspect for cells derived from indexed powder or single-crystal diffraction patterns, space group for cells derived from Rietveld refinements.
[2] Corrected for unit cell of NaCl standard in actualized Å units (original values were greater by a factor of 5.6404/5.6397).

so, however, an important ambiguity remains as to the absolute assignment of Si or Al to *T*1 (note that, for alternating Al–Si distribution, the assignment is defined by a sole tetrahedron). A solution to this problem came from ^{29}Si MAS NMR data, which reflect the *TOT* angles and were used to check the different alternatives issued from Rietveld refinement, much in the same way as better resolved diffraction data would have been used to establish the appropriate *TOT* angles. On the basis of the combined data, we can conclude that the Al–Si ordered *and* geometrically sound model has space group $P12_11$, and the orthorhombic symmetries $Pn2_1m$ and $P2_12_12_1$ must still be supergroups; $Pn2_1m$ is a well-approximated pseudosymmetry due to the similarity of Al and Si in X-ray-diffraction experiments, whereas $P2_12_12_1$ corresponds to the topochemical symmetry and may be a true supergroup that should be considered in phase transitions at high temperatures.

Role of synthesis conditions and occupancy of K

Substituted tridymite phases show remarkably diverse chemical compositions, mainly attributable to the intrinsic flexibility of the Al–O–Si linkage, which allows adaptation of the geometrically non-rigid frameworks in response to crystal-chemical influences. Superstructures are relatively easy to form, and there is much scope for order–disorder of framework

cations, and through the introduction of cavity cations and vacancies. With the addition of temperature- and pressure-driven displacive phase-transitions, the overall behavior becomes highly complex and intriguing.

In this work, the crystallization of $KAlSiO_4$-*O1* was accompanied by the formation of trace alumina. Therefore, compared with the "ideal" formula $KAlSiO_4$, the structure should contain an excess of Si at the expense of Al. Charge-balance is likely accomplished by a deficiency of potassium, leaving vacancies at the extra-framework cavity sites, according to the equation $K^+ + Al^{3+} \rightarrow \square + Si^{4+}$. Additional Rietveld calculations suggest indeed that the occupancy of K at some sites is less than 1 (*cf.* the high atomic displacement parameter in Table 3), and the results acquired by electron microscopy (Figs. 6 to 9) show extensive twinning, which might have its origin at interfaces where vacancies and excess Si accumulate and the Al–Si order inverts.

Support for such a mechanism comes from the ^{29}Si MAS NMR spectra in which a broad feature toward the right of the characteristic doublet of the $KAlSiO_4$-*O1* structure is observed (Fig. 4). This region contains the resonance peaks for Si in the configurations from $Si(Al_3Si)$ to $Si(Si_4)$, which are expected at increments of –5 ppm from –93 to –108 ppm, respectively. Twinning through accumulation of Si at interfaces can be represented by the formula $2Al_3Si–AlSi_3 \rightarrow Al_3Si–SiAl_3 + Si_3Al–SiSi_3$, and would have the net effect to create $Si(Al_3Si)$ and $Si(AlSi_3)$ configurations at the expense of $Si(Al_4)$, giving rise to peaks at –93 and –103 ppm in the ratio 5:1. In contrast to the more crystalline $KAlSiO_4$-*O1* sample, the polycrystalline sample prepared for the present study shows an important intensity at –93 ppm in accordance with a high frequency of such Si-rich interfaces. Additional work, including HRTEM studies of $KAlSiO_4$-*O1* samples of different origin, will be needed to resolve the subtle problems of twinning and pseudosymmetry.

Conclusions

The $KAlSiO_4$ polymorphs are substances of environmental significance. For example, in fluidized bed incinerators, the quartz sand can react with potassium-bearing wastes to produce clinkers that ultimately reduce the efficiency of waste reduction. Therefore, a more complete understanding of the phase diagram for the system $K_2O–Al_2O_3–SiO_2$ provides a starting point for controlling the ratio of waste feed to bed sand and other incineration parameters.

At lower temperatures (especially with longer firing times), alternative cells, all of them related to the tridymite subcell, were observed by X-ray diffraction. The dominant phase obtained at 1000°C is "orthorhombic" $KAlSiO_4$-*O1* (*a* 15.669 Å, *b* 9.057 Å, *c* 8.621 Å, β 90.16°), and its structure was successfully modeled by Rietveld refinement in the monoclinic space-group $P12_11$, which allows for alternating Al–Si order to comply with observed ^{29}Si MAS NMR spectroscopic data. Results from electron microscopy suggest also that the true symmetry is $P12_11$, but pseudosymmetry and twinning are extensive, which explains the difficulties encountered to establish the space group and crystal structure of "orthorhombic" $KAlSiO_4$ or $KAlSiO_4$-*O1*.

Acknowledgements

Joseph V. Smith was one of the first to recognize the singularity of the "orthorhombic" $KAlSiO_4$-*O1* phase and to establish its unit cell (1957, with O.F. Tuttle). He later resolved the first structure of a $KAlSiO_4$ polymorph (kalsilite; 1965, with A.J. Perrotta). On occasion of the International Conference on Molecular Sieves (1977), he became aware of the ongoing work on the crystal structure of $KAlSiO_4$-*O1* by one of us (MG). Very much interested in this structure, he eventually suggested, in his 1977 paper, that the polymorphs of $KAlSiO_4$ might be worth investigating in the search for new framework topologies based on two or more ring sequences. We are happy to be able to contribute this paper in his memory.

This work was supported through a joint NRC–A*STAR research program on "Advanced Ceramic Methods for the Co-stabilisation and Recycling of Incinerator Fly Ash with Industrial Wastes", research funds (60%) from the Italian Ministry (MURST–MIUR–MUR), and a research project on "Silicatos porosos para la preparación de membranas semipermeables: conductividad iónica y permeabilidad hidráulica en relación con la estructura cristalina" of CAICYT, Madrid. Thanks are due to guest editor Ross J. Angel and the editor for their continuing interest in this paper, as well as to S. Merlino and an anonymous reviewer for helpful criticism.

References

Andratschke, M., Range, K.J., Haase, H. & Klement, U. (1992): Die Kristallstruktur von α-$KZnPO_4$. *Z. Naturforsch.* **B47**,1249-1254.

Baur, W.H. (1974): The geometry of polyhedral distortions. Predictive relationships for the phosphate group. *Acta Crystallogr.* **B30**, 1195-1215.

Bonaccorsi, E., Merlino, S. & Pasero, M. (1988): Trikalsilite: its structural relationships with nepheline and tetrakalsilite. *Neues Jahrb. Mineral., Monatsh.*, 559-567.

Buerger, M.J. (1954): The stuffed derivatives of the silica structures. *Am. Mineral.* **39**, 600-614.

Capobianco, C. & Carpenter, M. (1989): Thermally induced changes in kalsilite ($KAlSiO_4$). *Am. Mineral.* **74**, 797-811.

CELLAI, D., BONAZZI, P. & CARPENTER, M.A. (1997): Natural kalsilite, $KAlSiO_4$, with *P*31*c* symmetry: crystal structure and twinning. *Am. Mineral.* **82**, 276-279.

CHEARY, R.W. & COELHO, A.A. (1998): Axial divergence in a conventional X-ray powder diffractometer. II. Realization and evaluation in a fundamental-parameter profile fitting procedure. *J. Appl. Crystallogr.* **31**, 862-868.

COOK, L.P., ROTH, R. S., PARKER, H. S. & NEGAS, T. (1977): The system K_2O–Al_2O_3–SiO_2. 1. Phases on the $KAlSiO_4$ –$KAlO_2$ join. *Am. Mineral.* **62**, 1180-1190.

ELFAKIR, A., SOURON, J.-P., WALLEZ, G., QUARTON, M. & TOUBOUL, M. (1998): Tl_2SO_4–Li_2SO_4 phase diagram and properties of $TlLiSO_4$. *Solid State Ionics* **110**, 145-151.

ENGELHARDT, G. & MICHEL, D. (1987): *High-Resolution Solid-State NMR of Silicates and Zeolites*. Wiley, Chichester, U.K.

GALLAGHER, S.A., MCCARTHY, G.J. & SMITH, D.K. (1977): Preparation and X-ray characterization of $CsAlSiO_4$. *Mater. Res. Bull.* **12**, 1183-1190.

GIBBS, R.E. (1927): The polymorphism of silicon dioxide and the structure of tridymite. *Proc. R. Soc. A. Math. Phys.* **113**, 351-368.

GREGORKIEWITZ, M. (1980): *Synthese und Charakterisierung poröser Silicate*. Dissertation, Technische Hochschule Darmstadt, Darmstadt, Germany.

GREGORKIEWITZ, M. (1986): Alkali ion diffusion in M'($AlSiO_4$) compounds with frameworks of the tridymite topology and its variants. *Solid State Ionics* **18–19**, 534-538.

GREGORKIEWITZ, M. & SCHÄFER, H. (1980): The structure of $KAlSiO_4$ kaliophilite-*O1*: application of the subgroup–supergroup relations to the quantitative space group determination of pseudosymmetric crystals. *Sixth Eur. Crystallographic Meeting* (*Barcelona*), 155 (abstr.).

HAHN, T. & BUERGER, M.J. (1955): The detailed structure of nepheline, $KNa_3Al_4Si_4O_{16}$. *Z. Kristallogr.* **106**, 308-338.

HAMILTON, W.C. (1965): Significance tests on the crystallographic R-factor. *Acta Crystallogr.* **18**, 502-510.

HAMMONDS, K.D., DOVE, M.T., GIDDY, A.P., HEINE, V. & WINKLER, B. (1996): Rigid unit phonon modes and structural phase transitions in framework silicates. *Am. Mineral.* **81**, 1057-1079.

HEANEY, P.J., PREWITT, C.T. & GIBBS, G.V., eds. (1994): Silica: Physical Behavior, Geochemistry, and Materials Applications. *Rev. Mineral.* **29**.

HENDERSON, C.M.B. & TAYLOR, D. (1988): The structural behaviour of the nepheline family. 3. Thermal expansion of kalsilite. *Mineral. Mag.* **52**, 708-711.

HÖRKNER, W. & MÜLLER-BUSCHBAUM, HK. (1979): Zur Kristallstruktur von $BaAl_2O_4$. *Z. Anorg. Allg. Chem.* **451**, 40-44.

HUTCHINGS, G.J., HUDSON, I.D. & TIMMS, D.G. (2004): Dehydration of 2-methylbutanal to isoprene using aluminium phosphate catalysts. *Chem. Mater. Sci.* **61**, 219-224.

INT. UNION CRYSTALLOGRAPHY CONGRESS (Ottawa) (1984): Recommended data for α-Al_2O_3 in $R\bar{3}c$ (rhombohedral setting). a = 5.12984 Å, α = 55.28333°, Al on 4*c* with x = 0.35227 and U_{ii} = 31.2 pm^2, O on 6e with x = 0.55626 and U_{ii} = 36.9 pm^2.

JIMÉNEZ-RIOBOO, R. & GREGORKIEWITZ, M. (1999): Alkali cation diffusion in the channel system of hexagonal nepheline $(K,Na,\square)Na_3[Al_3(Al,Si)Si_4O_{16}]$. *J. Electrochem. Soc.* **146**, 2620-2630.

KHOMYAKOV, A.P., NECHELYUSTOV, G.N., SOKOLOVA, E., BONACCORSI, E., MERLINO, S. & PASERO, M. (2002): Megakalsilite, a new polymorph of $KAlSiO_4$ from the Khibina alkaline massif, Kola Peninsula, Russia: mineral description and crystal structure. *Can. Mineral.* **40**, 961-970.

KIHARA, K. (1978): Thermal change in unit-cell dimensions, and a hexagonal structure of tridymite. *Z. Kristallogr.* **148**, 237-253.

KLASKA, R. & JARCHOW, O. (1975): Die Kristallstruktur und die Verzwillingung von $RbAlSiO_4$. *Z. Kristallogr.* **142**, 225-238.

KUNIMOTO, T., HONMA, T., YAMANE, A., SHAO, Y.L., KAKEHI, K.N., OHMI, K. & KOBAYASHI, H. (2007): Study on X-ray absorption near edge structure of Eu centers in $CaAl_2O_4$: Eu phosphor thin films prepared by pulsed laser deposition. *Jap. J. Appl. Phys.* **46**, 5874-5878.

KUNZE, G. (1954): Über die rhombische Modification von $KAlSiO_4$ in Anlehnung an den Kalsilit. *Heidelberger Beitr. Mineral. Petrogr.* **4**, 99-129.

LARSON, A.C. & VON DREELE, R.B. (1998): *GSAS General Structure Analysis System*. Los Alamos National Laboratory, Los Alamos, New Mexico.

LI, YING, LAURSEN, K., WHITE, T.J. & GREGORKIEWITZ, M. (2003): The crystal chemistry and microstructure of fluidised bed incinerator clinker tridymite. *J. Mater. Eng.* **14**, 119-125.

LIEBAU, F. (1985): *Structural Chemistry of Silicates*. Springer-Verlag, Berlin, Germany.

LOEWENSTEIN, W. (1954): The distribution of aluminum in the tetrahedra of silicates and aluminates. *Am. Mineral.* **39**, 92-96.

MADANI, A., AZNAR, A., SANZ, J. & SERRATOSA, J.M. (1990): ^{29}Si and ^{27}Al NMR study of zeolite formation from alkali-leached kaolinites. Influence of thermal preactivation. *J. Phys. Chem.* **94**, 760-765.

McConnell, J.D.C. (1962): Electron diffraction study of subsidiary maxima of scattered intensity in nepheline. *Mineral. Mag.* **33**, 114-125.

Merlino, S. (1984): Feldspathoids: their average and real structures. *In* Feldspars and Feldspathoids (W.L. Brown, ed.). Reidel Publishing Company, Dordrecht, The Netherlands (435-470).

Merlino, S., Franco, E., Mattia, C.A., Pasero, M. & DeGennaro, M. (1985): The crystal structure of panunzite (natural tetrakalsilite). *Neues Jahrb. Mineral., Monatsh.*, 322-328.

Minor, D.B., Roth, R.S., Brower, W.S. & McDaniel, C.L. (1978): Alkali ion exchange reactions with $RbAlSiO_4$: a new metastable polymorph of $KAlSiO_4$. *Mater. Res. Bull.* **13**, 575-581.

Nayak, M. & Kutty, T.R.N. (1996): Large range of nonstoichiometry in barium ortho aluminate prepared through gel-to-crystallite conversion. *Mater. Res. Bull.* **31**, 227-234.

Newsam, J. M. (1987): Silicon-29 chemical shifts in sodalite materials. *J. Phys. Chem.* **91**, 1259-1262.

Norby, P. & Fjellvåg, H. (1992): Preparation, structural and thermal properties of $MAlSiO_4$ (M = Li,Na,K,Rb,Cs,Tl,Ag) of ABW type. *Zeolites* **12**, 898-908.

Nukui, A., Nakazawa, A.H. & Akao, M. (1978): Thermal changes in monoclinic tridymite. *Am. Mineral.* **63**, 1252-1259.

Palmer, D.C. (1994): Stuffed derivatives of the silica polymorphs. *In* Silica: Physical Behavior, Geochemistry, and Materials Applications (P.J. Heaney, C.T. Prewitt & G.V. Gibbs, eds.). *Rev. Mineral.* **29**, 83-118.

Perrotta, A.J. & Smith, J.V. (1965): The crystal structure of kalsilite, $KAlSiO_4$. *Mineral. Mag.* **35**, 588-595.

Rigby, G.R. & Richardson, H.M. (1947): The occurrence of artificial kalsilite and allied potassium aluminum silicates in blast-furnace linings. *Mineral. Mag.* **28**, 75-88.

Sandomirsky, P.A. & Urusov, V.S. (1988): Phase relationships and thermal expansion for $KAlSiO_4$ polymorphs. *Geochem. Int.* **25**, 62-72.

Shi, J., Anderson, M.W. & Carr, S.W. (1996): Direct observation of zeolite A synthesis by in situ solid-state NMR. *Chem. Mater.* **8**, 369-375.

Smith, J.V. (1977): Enumeration of 4-connected 3-dimensional nets and classification of framework silicates. I. Perpendicular linkage from simple hexagonal net. *Am. Mineral.* **62**, 703-709.

Smith, J.V. & Tuttle, O.F. (1957): The nepheline–kalsilite system. I. X-ray data for the crystalline phases. *Am. J. Sci.* **255**, 282-305.

Sobrados de la Plaza, I. (1991): *Síntesis, cambio iónico y conductividad de electrolitos sólidos de la familia de los tectosilicatos M[AlSiO4] (M=Li,Na,K,Ag).* Tesis doctoral, Facultad de Ciencias Químicas, Universidad Complutense, Madrid, Spain.

Stebbins, J.F., Murdoch, J.B., Carmichael, I.S.E. & Pines, A. (1986): Defects and short range order in nepheline group minerals: a silicon-29 nuclear magnetic resonance study. *Phys. Chem. Minerals* **13**, 371-381.

Topas V3 (2005): *General Profile and Structure Analysis Software for Powder Diffraction Data.* Bruker AXS, Karlsruhe, Germany.

Vinograd, V.L. (1996): Computer simulations of the Al–Si disorder in synthetic cordierites: configurational entropy constrained by ^{29}Si NMR data. *Phys. Chem. Minerals* **23**, 391-401.

Wallez, G., Lucas, F., Souron, J.P. & Quarton, M. (1999): Potassium–zinc monophosphate: an original polymorphic tridymite derivate. *Mater. Res. Bull.* **34**, 1251-1261.

Xu, Huifang & Veblen, D.R. (1996): Superstructures and domain structures in natural and synthetic kalsilite. *Am. Mineral.* **81**, 1360-1370.

Received November 21, 2007, revised manuscript accepted December 31, 2008.